Transaction B: Mechanical Engineering
Vol. 16, No. 6, pp. 534–544

Research Note

SCIENTIA
IRANICA

Investigations of Supersonic Flow Around a Long Axisymmetric Body

M.R. Heidari[1,*], M. Farahani[2], M.R. Soltani[2] and M. Taeibi-Rahni[2]

Abstract. *In this work, a supersonic turbulent flow over a long axisymmetric body was investigated, both experimentally and computationally. The experimental study consisted of a series of wind tunnel tests for the flow over an ogive-cylinder body at a Mach number of 1.6 and at a Reynolds number of* 8×10^6*, at angles of attack between -2 and 6 degrees. It included the surface static pressure and the boundary layer profile measurements. Further, the flow around the model was visualized using a Schlieren technique. All tests were conducted in the trisonic wind tunnel of the Qadr Research Center (QRC). Also, the same flow at zero angle of attack was computationally simulated using a multi-block grid (with patched method around the block interfaces) to solve the thin layer Navier-Stokes (TLNS) equations. The numerical scheme used was implicit Beam and Warming central differencing, while a Baldwin-Lomax turbulence model was used to close the Reynolds Averaged Navier-Stokes (RANS) equations. The static surface pressure results show that the circumferential pressure at different nose sections varies significantly with angle of attack (in contrast to the circumferential pressure signatures along the cylindrical part of the body), while the total pressure measurements in the boundary layer vary significantly both radially and longitudinally. Two belts with various leading edge angles were installed at different locations along the cylindrical portion of the model. The computational results obtained were compared with some experimental ones (found by these authors), showing considerably close agreements.*

Keywords: *Supersonic flow; Pressure distribution; Boundary layer; Long axisymmetric body; Multi-block; TLNS equations.*

INTRODUCTION

One of the most important parameters affecting missile length and diameter is the required space for their apparatus and systems, etc. Increasing this space causes an increase in both the body length and the missile fineness ratio (L/d) [1]. For such bodies, the problems of flow separation and boundary layer growth under various flight conditions are very important. Of course, the boundary layer growth and its separation affect the aerodynamic characteristics, particularly the drag force and the stability criterion. Both of these have important roles in missile performance and mission implementations. Also, the performance of various control surfaces (especially those located close to the end of the body) varies with flow separation [2].

For some rockets and missiles, the after body cross-section changes longitudinally (particularly in space vehicles). Furthermore, due to the lack of sufficient space for arranging the systems (e.g., actuator of controlled fins, avionics, etc.), it is necessary to increase the body cross section near those systems. The lack of space may also appear when controlled fins are installed on the motor surface. Hence, on many occasions, the body cross-section needs to be increased [3,4].

However, computation of flow parameters and their variations for non-zero angles of attack, when bodies are tapered, is not an easy task, e.g. it takes a considerable amount of memory and CPU time to compute the flow over such bodies. In addition, as the angle of attack increases, the flow over a portion of the body may separate, making the flow more complicated. Moreover, experimental data for flow properties along tapered bodies to validate CFD codes are rare [4,5].

1. *Space Research Institute, 26th km of Tehran-Karaj Highway, Tehran, Iran.*
2. *Department of Aerospace Engineering, Sharif University of Technology, Tehran, P.O. Box 11155-8639, Iran.*
*. *Corresponding author. E-mail: mrezaheidari@yahoo.com*

Received 22 June 2008; received in revised form 18 April 2009; accepted 6 June 2009

The computational simulation of flow over complex geometries usually requires structured multi-block grids. On the other hand, geometric complexity requires more blocks and also more grid points. Even though the computer programming (using multi-block grid for such flows) is very troublesome, it is computationally very efficient and quick. Also, suitable grid generation plays the first and most important role when using a multi-block grid.

Grid generation needs to be consistent with flow solution. In some methods, the discretization error increases due to the inaccurate adoption of grid boundaries with real flow boundaries, which could be due to the non-orthogonality of the grid lines, especially near the walls.

There has been much research performed in the areas of generation and use of multi-block grids, grid generation techniques, data management methods in different blocks and the production of grid generation software, which optimally require less trained users and quicker grid generation (especially for complex geometries) [6,7].

The different steps to compute flow using a multi-block grid are:

1. Geometric recognition and setting a suitable block structure;
2. Grid generation inside each block and finding the nodes on the block boundaries;
3. Solving the flow inside each block and then in the whole domain.

Also, multi-block grid generation has four steps, namely dividing the flow domain into different blocks, determining the exact geometric characteristics of each block, grid generation in each block and optimization of the overall grid [8]. The situation and location of boundaries between blocks are very important and thus inefficient structuring can lead to a divergence in the overall solution. Flow physics, such as shock waves and separated flow regions, determine the required number of blocks and how they are distributed.

In the present work, a series of wind tunnel tests on a long axisymmetric body were performed to investigate pressure distribution, the boundary layer profile and other flow characteristics at various angles of attack and at a constant supersonic Mach number of 1.6. Because of the low maneuverability of high fineness ratio missiles, the range of angles of attack for the present study was chosen to be moderate. Then, the effects of cross sectional area variations on surface static pressure distribution and on the boundary layer profiles were thoroughly investigated. This was performed by installing two belts (strips) having different cut-off angles on the cylindrical portion of the model. One of these belts was installed at the beginning of the after body part ($x/d = 7.5$), while the other was located near the end ($x/d = 13.25$). By changing the belt leading edge angles, different bodies were generated and thus the effects of varying the body cross-section were studied.

In the numerical part of this work, a stationary turbulent supersonic axisymmetric flow over the same body at zero angle of attack (in the absence of body forces and heat sources) was investigated using the computer code developed in this work (MBTLNS). An adiabatic wall with negligible variations of the viscous fluxes in the streamwise direction was assumed. Also, the flow domain was blocked in a streamwise direction and a patched method was used in the block boundaries. In each block, the Thin Layer Navier-Stokes (TLNS) equations were solved, using the implicit delta form finite difference method with the Beam and Warming central differencing scheme [9]. For turbulence modeling, the algebraic two-layer Baldwin-Lomax model was used and the shock waves were captured using a shock capturing technique. At each iteration of the overall solution, the flow domain is swept from the first block at the nose to the last block at the end of the body. The computational results for zero angle of attack, Mach number of 1.6 and Reynolds number of 8×10^6, for flow over an axisymmetric ogive-cylinder with two sets of strips with angles 5 and 15 degrees, were compared with the related experimental results obtained in this work. The most important ability of the present software is that it can solve the flow around complex geometries, using a personal computer with a relatively small memory.

EXPERIMENTAL EQUIPMENT AND TESTS

All tests were conducted in the trisonic wind tunnel of QRC. The equipment used for this investigation includes: Schlieren visualization system, A/D board, traversing mechanism, rake, vacuum pump, manometer, pressure transducer, multiplexer board, computer and data acquisition software.

The QRC wind tunnel is an open-circuit blow down tunnel and operates continuously between Mach numbers 0.4-2.2, via engine RPM and nozzle adjustments. It has a test section of $60 \times 60 \times 120$ cm^3 and is equipped with various internal strain gauge balances for force and moment measurements, pressure transducers, Schlieren visualization system and etc. [10].

The model used in this study had a fineness ratio of 2.5, a circular-arc and ogival nose tangent to a cylindrical after body with $L/d = 15$ (Figure 1a). It was equipped with 36 static pressure ports located both longitudinally and circumferentially. To study the effects of cross section changes, two belts with various leading edge angles were installed on the model

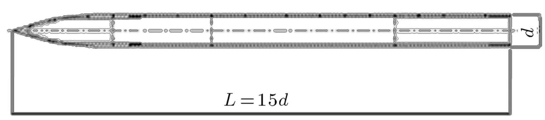

(a) Simple model

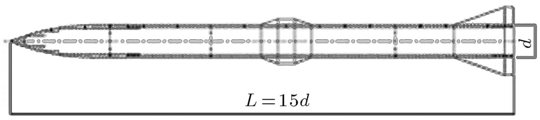

(b) Model with belt

Figure 1. Schematic of different models used.

(Figure 1b). Here, the first model is used when talking about the main or simple model (the one without belts), the second model for the one with (5, 5) degree belts and the third model for the one with (15, 12) degree belts.

The traversing mechanism which was designed and built particularly for this study is capable of moving the rake perpendicular to the body axis with small steps of about 0.003 mm in a z direction. This system was installed on the α-mechanism base, such that the tubes (pitot total pressure) of the rake were always parallel to the model. Note that the entire traversing mechanism was fully controlled by a computer.

Various tests were conducted to study the flow characteristics along the model. The free stream Mach number was 1.6, while the angle of attack was varied between -2 and 6 degrees. At each angle of attack and for all models, the rake at several longitudinal stations for at least 11 locations in a z direction obtained the total pressure data. An accurate linear potentiometer was used to determine the distances between the body surface and the rake. Note that all experimental data shown here are the ensemble average of several hundred data taken several times to ensure repeatability.

GOVERNING EQUATIONS AND COMPUTATIONAL METHODOLOGY

In the present study, a turbulent supersonic flow over a long axisymmetric body at zero angle of attack was computationally simulated. The Reynolds averaged TLNS equations were solved using Beam and Warming central differencing and the Baldwin-Lomax turbulence model. This model is frequently used, because of its simplicity and reliability. Even though in some flow situations it is up to about 10% less accurate compared to some other models, it can reduce the amount of computation up to about 50%.

The first step in grid generation is the correct nodal distribution along the body surface. Then, is the blocking of the domain and finally, comes the grid generation inside each block. Since we are not ignoring viscosity, a much finer grid is required near the surfaces. Also, a finer grid is required in the block, which may contain shock waves, flow separation, or other high flow gradient regions. For most blocks, where there are relatively simple geometries, algebraic grid generation is usually used.

The location of block interfaces is very important. In this work, the blocks were structured in a streamwise direction. For blocking of the domain, one needs to first estimate different flow phenomena and the complexity of the body geometry, which may be encountered. Then, the block interfaces are located. Here, we used a connected and disconnected uniform patched method at the interfaces. Note that whenever connected meshes are used, the lines from one block are continued into the next block. This way, interpolation is not usually required at the interfaces. Besides the limitations this may bring along, it eliminates the errors due to non-conservative data along the interfaces.

Even when a continuous grid (same grid type in each block) is used, any sudden change along the block interfaces (such as angles between the lines of the two neighboring blocks) may cause a drastic discontinuity of the grid transformation metrics. On the other hand, for a more accurate application of the wall boundary conditions and the flow solutions in each block, it may be required to increase the number of nodes and the grid lines especially in the direction perpendicular to the wall. This usually leads to a disconnected grid at the interfaces. Mostly, this is done by halving or doubling the grid points in the blocks neighboring the interfaces [11].

In each block, the boundary conditions and the information received from the neighboring blocks affect the flow solution. Thus, any error related to the transfer of information within the blocks directly affects the solution in each block, the overall solution and its convergence. Therefore, we need to use interpolation techniques at the interfaces with the least error, which is preferably conserved.

In the present work, a suitable linear interpolation technique was used for computations at points of a block extended into the neighboring block. Thus, the distribution of lines in the left and the right sides of the interfaces is quite arbitrary and without any limitations. After breaking down the flow domain into several blocks, the information set for each block is obtained. This set includes the block number, the interface numbers and types, the geometric locations of the corners of each block and the numbers and type of the neighboring interfaces. Also, other internal information of each block, such as the number of nodes and their arrangement, the CFL number and the artificial viscosity coefficient, etc. has to be known before the flow solution is performed.

Even though the solution may be converged in each block, the overall solution may well be diverged. This difficulty mainly arises from the inappropriate ordering of the solution procedure for different blocks which needs to be simple and smooth. Also, it is very important that different flow variables have the same weight and harmony. In this work, using a simple and suitable procedure, we start from the first block at the nose which contains the upstream inflow information, and pass through the chain of the blocks until we reach the last one located at the end of the body, containing the outflow information. In each block, the solution is only performed in one time step. Note that if we were having any type of iteration in any block, it should be harmonized with the other blocks especially neighboring ones. This is a considerably difficult task and can lead to convergence problems of the overall solution.

Here, the solution accuracy has been compared to the single block case. As far as the convergence speed is concerned, different parameters, such as the numbering and arrangement of the nodes, the CFL number, the initial conditions, the time step, the artificial viscosity coefficient, etc. for each block and the position and type of block interface, have been thoroughly investigated and evaluated.

RESULTS AND DISCUSSION

A supersonic turbulent flow over a long axisymmetric body was investigated both experimentally and computationally. The experimental study consisted of a series of wind tunnel tests for the flow over an ogive-cylinder body at Mach number of 1.6 and at angles of attack between -2 and 6 degrees. To study the effects of cross section variations on pressure distribution and boundary layer profiles, several belts with various leading edge angles were installed at different locations along the cylindrical portion of the model. The wind tunnel tests included the surface static pressure and boundary layer profile measurements. Further, the flow around the model was visualized using the Schlieren technique. All tests were conducted in the QRC's trisonic wind tunnel. On the other hand, for the above body, a 1.6 Mach number and a 8×10^6 Reynolds number flow at zero angle of attack was computationally investigated, using a multi-block grid (with patched method around the block interfaces) to solve the TLNS equations. The numerical scheme used was implicit Beam and Warming central differencing, while a Baldwin-Lomax turbulence model was used to close the RANS equations.

First, at various angles of attack, the Schlieren visualization technique was used to study the shape of the shocks formed around the model nose and places where the area changed (and their variations with angle of attack). Figure 2 shows the shock waves as well as the expansion waves on the large strip at zero angle of attack. The related numerical results are also shown there for comparison purposes. From this figure, it is seen by inspection that there exists relatively close correlations between the numerical and experimental results for both cases.

Figure 3 shows the shock wave formed in front of the model and ahead and behind the belt used for varying the model cross section at a 6 degree angle of attack. It is seen from this figure that the shock wave is not symmetric, resulting in a lower strength on the leeward side of the model and also causing higher pressure on the windward portion of the nose and lower pressure on its leeward side (thus a normal force is generated). Figure 3b clearly shows the oblique shock,

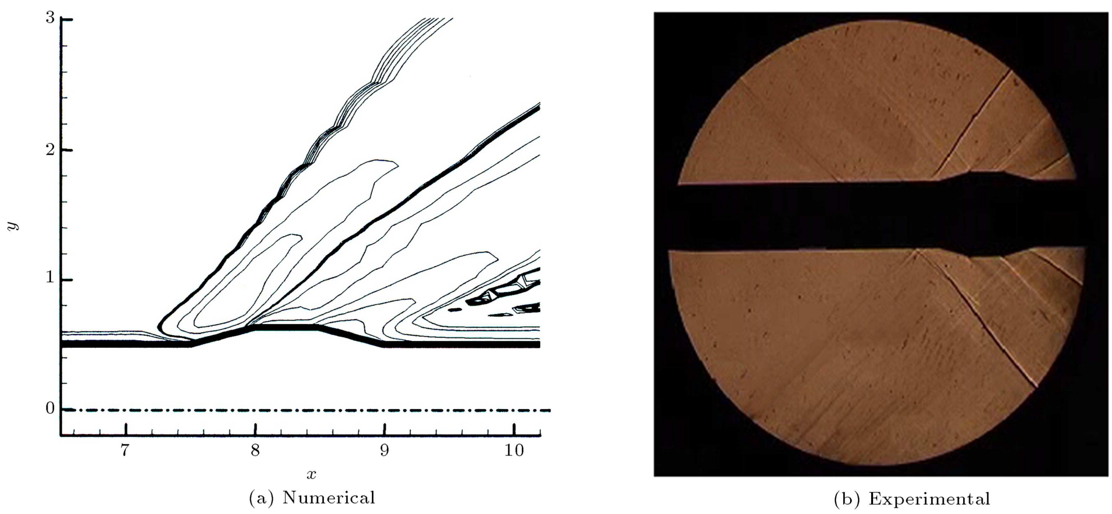

(a) Numerical (b) Experimental

Figure 2. Experimental and numerical flow field over the model with large belt (15°) at $\alpha = 0$.

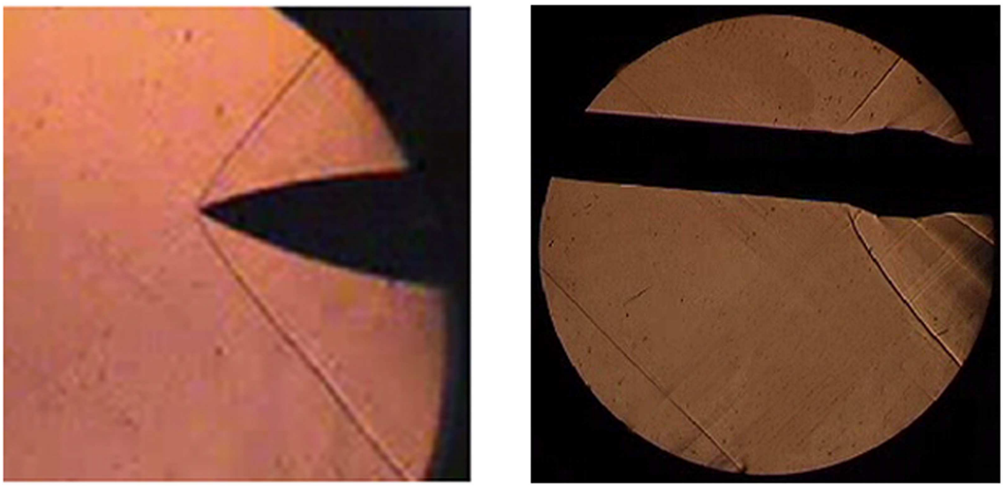

(a) Oblique shock in the nose region of the model

(b) Compression and expansion waves around the large belt (15°)

Figure 3. Schlieren photograph illustrating the shock formation at $\alpha = 6°$.

as well as the expansion waves, formed in the front and on the surface of the belt installed at $x/d = 7.5$. Furthermore, the oblique shock formed behind the belt, to reduce flow velocity and turn it parallel to the model surface, is clearly visible in this figure. Again, the strengths and shapes of the upper and lower shock formed ahead of the belt are not the same.

Figure 4 shows longitudinal static pressure distribution over the model surface. Figure 4a compares our experimental and CFD results for zero angle of attack, while Figure 4b compares our experimental results with theoretical ones (SOSE; Second Order Shock Expantion [12]) for 4 and 6 degree angles of attack. Note that the measurement errors are calculated and shown in Figure 5b. From these figures it is clearly seen that all three methods predict the surface pressure very closely for $0 < L/d < 12$ at $\alpha = 0$ degrees. From Figure 4b the experimental and theoretical data compare well up to about $x/d = 12$. The differences are probably due to the base flow affecting the boundary layer on the model surface near its end. Note that by increasing the angle of attack, the pressure taps located at a zero circumferential angle ($\theta = 0$) will be located at the leeward side of the model. Therefore, their static pressure should decrease. These pressure losses are, however, considerable only along the nose section of the body. This confirms that, for axisymmetric bodies, the contribution of the nose in generating the lift force is greater than that of its after body portion [13-15]. Increasing α from 4 to 6 degrees has small effects along the nose section.

The experimental and theoretical circumferential pressure data at $x/d = 3$ and 11.5 for 4 and 6 degree angles of attack are shown in Figure 5. For the first station, by increasing the angle of attack, C_p increases slightly at the windward side, as expected.

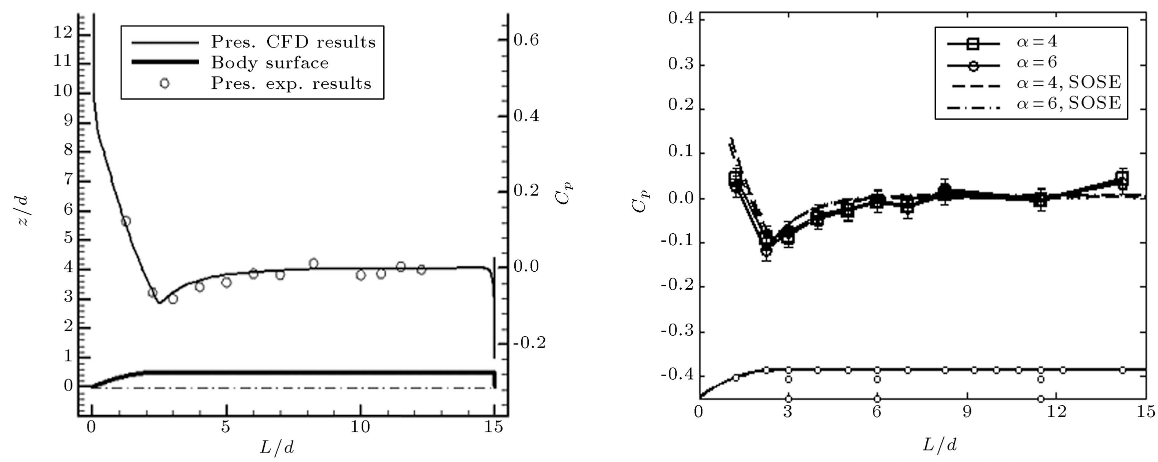

(a) $\alpha = 0$

(b) $\theta = 4°$ and $6°$

Figure 4. Comparison of experimental, theoretical, and numerical longitudinal pressure distribution.

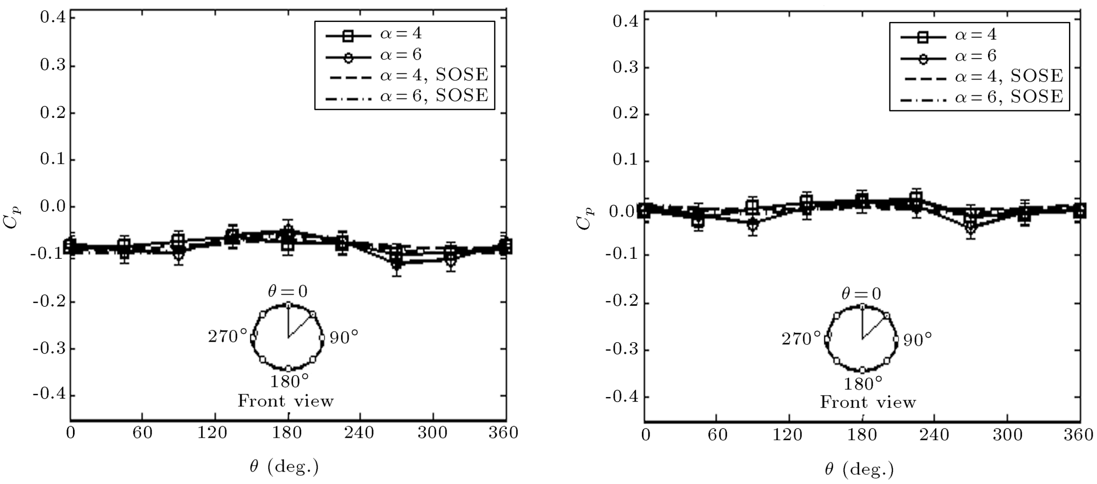

(a) $x/d = 3$ (b) $x/d = 11.5$

Figure 5. Comparison of experimental and theoretical circumferential pressure distribution at $\alpha = 4°$ and $6°$.

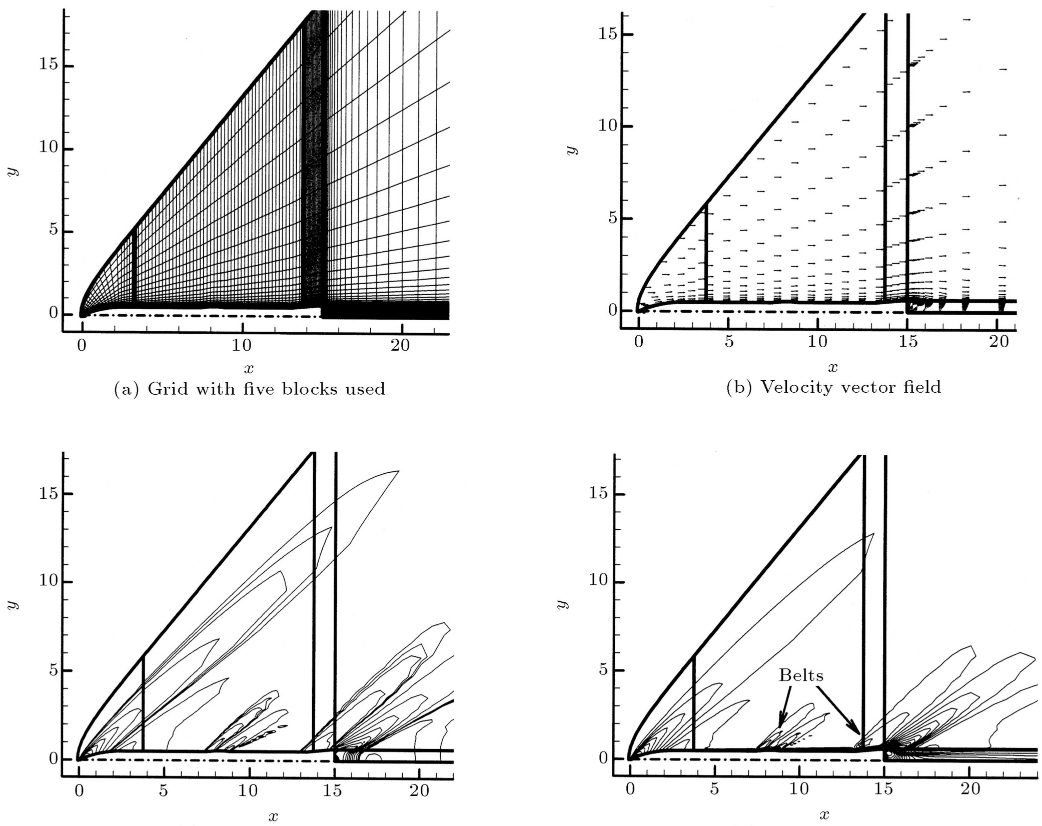

(a) Grid with five blocks used (b) Velocity vector field (c) Pressure contours (d) Density contours

Figure 6. Flow around the model with small 5° belt.

As α increases, the vortices separate from the nose and extend to the end of the body. These vortices are, in general, asymmetric and cause asymmetry of the circumferential pressure distribution on the leeward side of the body [12] (Figure 5b). In addition, the sensitivity of the model installation is high, due to its large fineness ratio; hence, a small error can cause a considerable sideslip angle. Note that the flow field study showed that the flow also has a small yaw angle [10].

Figure 6 shows the grid, the velocity vector field and the pressure and density contours for flow over the small belt model at a zero angle of attack, a Mach number of 1.6 and a Reynolds number of 8×10^6 (described before). Note that the flow domain has been broken into five blocks. Also, note from the

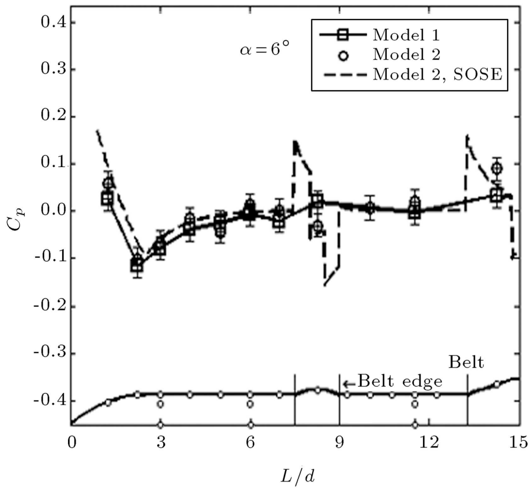

(a) Experimental, theoretical and numerical longitudinal pressure distribution

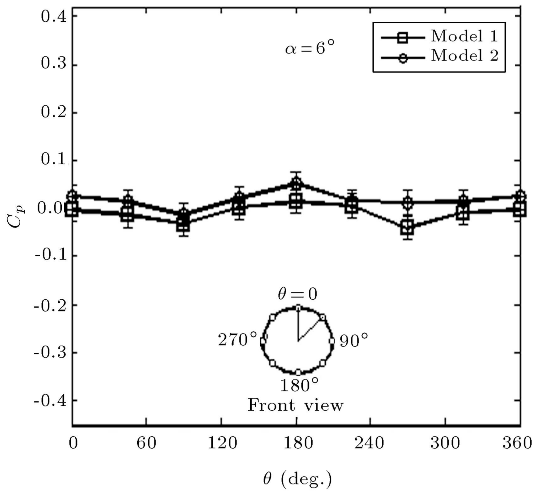

(b) Circumferential pressure distributions behind the middle belt ($x/d = 11.5$)

Figure 7. Effect of cross section variations on the model pressure distribution (model 2).

Table 1. The drag coefficients for the three cases studied.

Model	**Middle Belt Angle (Deg.)**	**End Belt Angle (Deg.)**	**Wave Drag**	**Friction Drag**
Body alone	-	-	0.146	0.077
Body with small belts	5	5	0.223	0.071
Body with big belts	15	12	0.776	0.068

pressure and the density contours that the solution is very smooth and continuous at block interfaces. In all these solutions the optimal grid has been determined and used. Also, note that the bow shock near the body nose has been captured with suitable accuracy and other flow shock and expansion waves along with flow vortices have been shown near the belts.

The effect of varying the model cross section (by adding belts with different leading edge angles) and the circumferential pressure distribution at 6 degree angles of attack are shown in Figure 7. The computational drag coefficient is obtained from the viscosity and pressure gradient effects on the body surface. Here, the longitudinal pressure distribution for both numerical and theoretical predictions compared well with experimental data up to the location where the model frontal area was changed via the belt. Behind the belt, however, all results are almost identical. The presence of the belt increases the longitudinal surface pressure by formation of an oblique shock, as seen in Figure 3b, over the inclined part of the belt. However, around the surface of the belt and behind it, the pressure decreases due to the formation of expansion waves (also seen in Figure 3b). The results of the circumferential pressure distributions show that sudden changes in cross sectional area have small effects on the pressure distribution around the perimeter of the model behind the belt (Figure 7b).

The drag coefficient is obtained from shear viscosity and pressure gradient effects on the body surface. In this work, for the small belt model, a wave drag of 0.223, a friction drag of 0.071 and a base drag of 0.369 have been computed (thus the total drag was 0.663). The drag coefficients for all models are shown in Table 1.

The computational and experimental boundary layer profiles for the simple model (uniform cross section) were compared at three different longitudinal stations and at zero angles of attack in Figure 8. From this figure, the agreements of data are relatively close, particularly for $z < 7$ mm.

Figure 9 shows the boundary layer profiles above the model at three different stations: $x/d = 2.75$, 5.75 and 11.25, for two different angles of attack (0 and 6 degrees). From this figure, it is clearly seen that the boundary layer thickness increases with x/d. Further, this figure shows that for $x/d = 2.75$ and at $\alpha = 6^\circ$ the velocity at the edge of the boundary layer ($z \cong 5$mm) is slightly higher than that outside of it ($z \cong 18$ mm). While for other locations ($x/d = 5.75$ and 11.25), the velocity outside the boundary layer never reaches that of V_∞ at $M_\infty = 1.6$. The increased velocity at the boundary layer edge is related to the

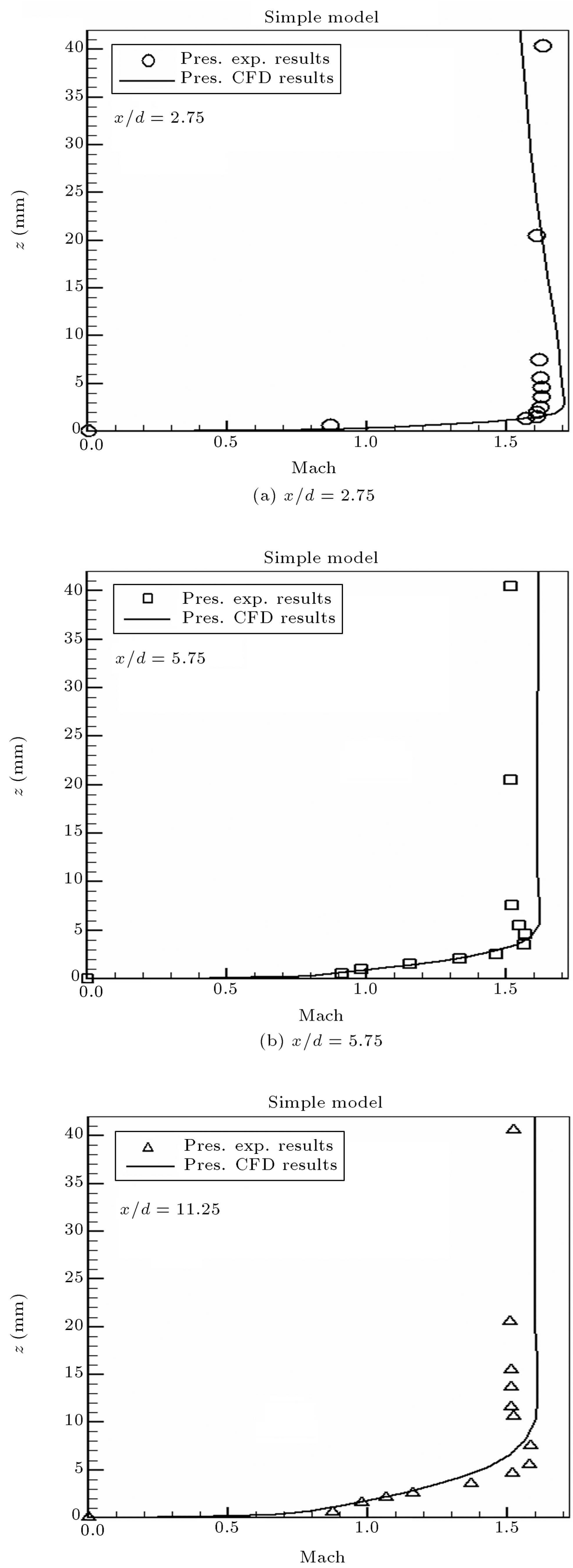

(a) $x/d = 2.75$

(b) $x/d = 5.75$

(c) $x/d = 11.25$

Figure 8. Experimental and numerical boundary layer profiles for simple model at $\alpha = 0$.

increase in the mass flow rate at the outer portion of the boundary layer due to velocity reduction in the inner layers (entrainment). Since the decrease in velocity inside the boundary layer causes a lower mass flow rate there, it must be compensated by an increase in velocity at the edge of the boundary layer. At $\alpha = 6°$ and at $x/d = 11.25$, the value of $\partial M/\partial z$ is different in comparison with the other data shown in Figure 9b. This change is probably due to the separation of the body vortices [16]. Moreover, the growth of the boundary layer at $x/d = 11.25$ is greater than that of the other stations (e.g., $x/d = 2.75$ and 5.75). Note that for all three stations as x increases the boundary layer thickness increases considerably. However, the increase in velocity at the boundary layer edge decreases marginally. This increase is due to the growth of the momentum layer thickness, δ^*, which permits the required mass flow rate through the boundary layer [14].

The variations of experimental boundary layer Mach numbers for the simple model, at $x/d = 5.75$ and 11.25 (at various angles of attack), are shown in Figure 10. At $x/d = 5.75$, with increasing the angle of attack, the boundary layer thickness grows. However, a slight increase in the boundary layer thickness is noted for small angles of attack. At higher angles of attack, the boundary layer thickness decreases appreciably for $x/d = 11.25$. It is presumed that the boundary layer fluid is shifted to form a pair of vortices along the sides of the model at large α, hence, reducing the boundary layer thickness.

The comparison of numerical and experimental boundary layer profiles over model 2, ahead and behind the middle belt at a zero angle of attack, is shown in Figure 11. This data compares relatively well, especially for $x/d = 5.75$. Note that the differences between the CFD and experimental results obtained are, at most, 15%. However, it is noted that such difference is much less (less than 7%) in other figures.

The variations of the experimental Mach number in the boundary layer for model 3 at $x/d = 11.25$, at various angles of attack, are presented in Figure 12. The trends of the boundary layer profiles for this model are the same as the simple model (Figure 10b). With increasing the angle of attack up to 2°, a slight increase in the boundary layer thickness is noted, while at higher angles of attack, the boundary layer thickness decreases appreciably. Note that the presence of the belts has almost no effect on the variations of the boundary layer profiles with angle of attack.

CONCLUSIONS

An extensive experimental study on a long axisymmetric tapered body in a turbulent supersonic flow was

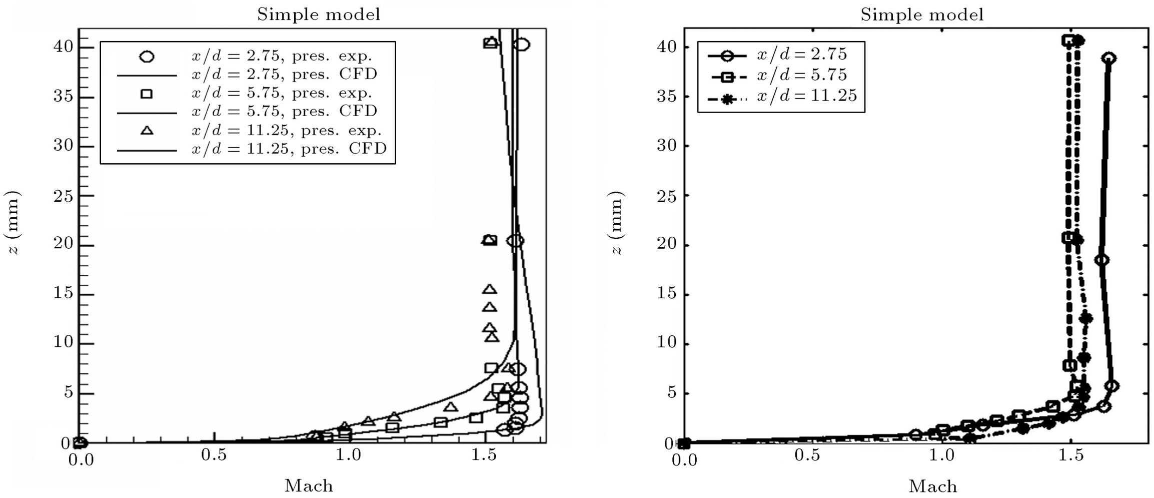

(a) $\alpha = 0°$ (b) $\alpha = 6°$

Figure 9. Comparison of the boundary layer profiles around the body.

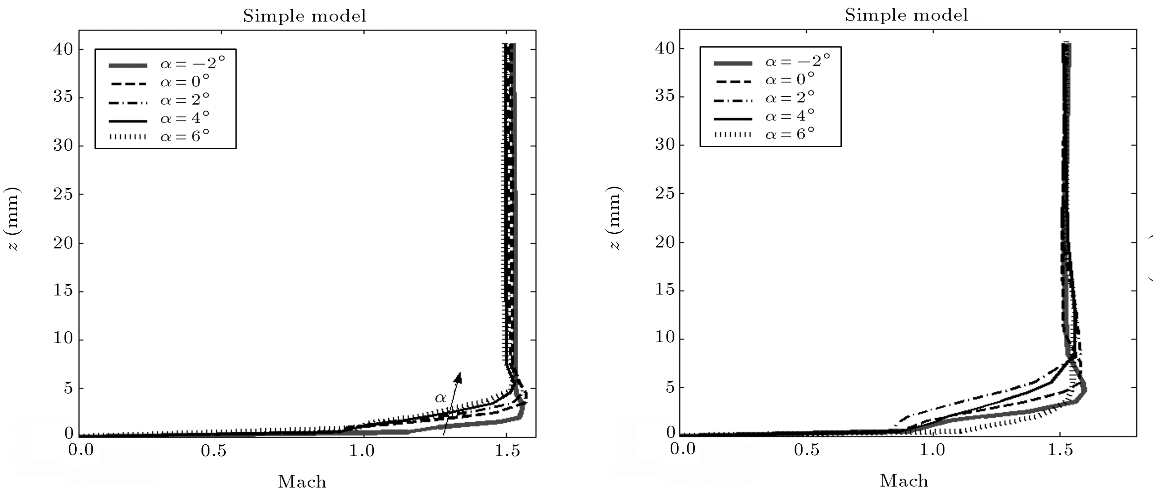

(a) $x/d = 5.75$ (b) $x/d = 11.25$

Figure 10. Effects of angle of attack on boundary layer profiles.

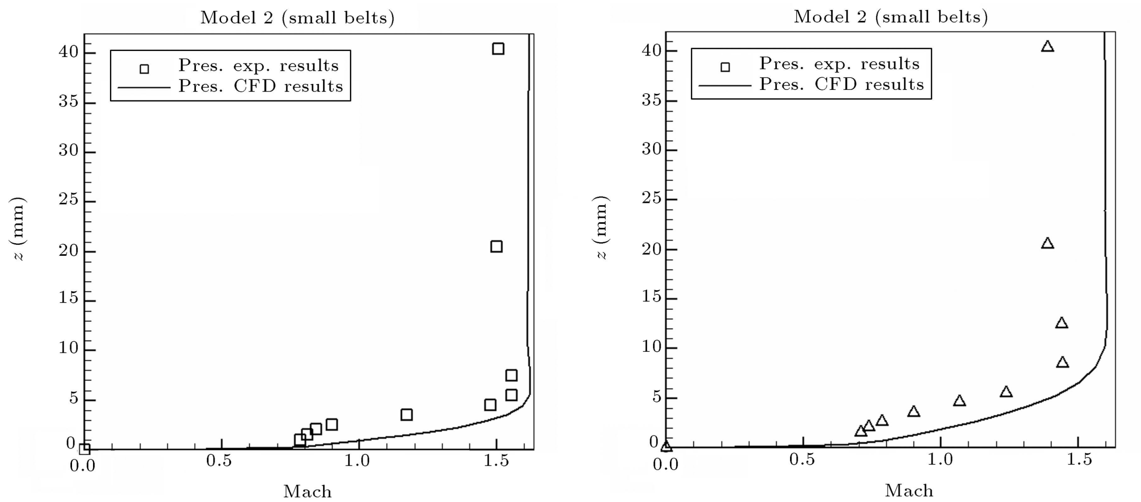

(a) $x/d = 5.75$, ahead of the middle belt (b) $x/d = 11.25$, behind the middle belt

Figure 11. Experimental and numerical boundary layer profiles for model 2 at $\alpha = 0$.

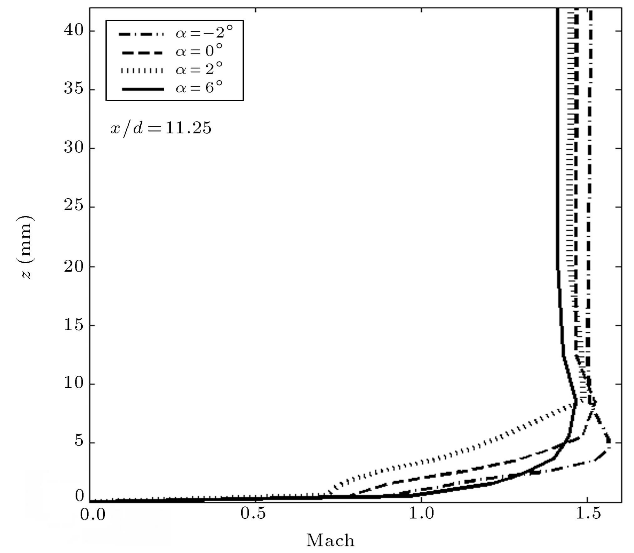

Figure 12. The effects of angle of attack on boundary layer profiles for model 3.

performed to mainly investigate pressure distributions and boundary layer profiles at various angles of attack. In order to study the effects of the model cross section variations, several belts with various leading edge angles were installed at different locations along the cylindrical portion of the model. In addition, the same flow at a zero angle of attack, using a structured multi-block grid (with patched method at the block interfaces) and the Baldwin-Lomax turbulence model solving the TLNS equations was computationally simulated.

The experimental static surface pressure results show that the circumferential pressure at different nose sections varies significantly with angle of attack (in contrast to the circumferential pressure signatures along the cylindrical part of the body). On the other hand, the total pressure measurements in the boundary layer vary significantly both radially and longitudinally.

Also, the experimental results obtained indicate that the installation of the belts with various leading edge angles has little effect on the pressure distributions along the forebody, while it has considerable effect on the after body pressure signatures. Also, the belts affect the boundary layer profiles, increasing their thicknesses and changing their shapes. Note that, for the models with belts, the value of $\partial M/\partial z$ at $z = 0$ is considerably different.

The computational results obtained were compared to some of our related experimental data showing relatively close agreements. Note that, at the block interfaces, there are not shown to be any noticeable discontinuities. Also, the flow shock and expansion waves are clearly shown in our numerical results and the computational shock angles compared well with the Schlieren results. These indicate the suitable accuracy of our numerical methodology. The Mach number contours at 6° angles of attack showed vortices at the end of the body. It seems that the addition of the belts increases the strength of these vortices and makes them more symmetric. It was also demonstrated that, for the same number of grid points, the single block case requires much more memory than multi-block cases. The MBTLNS computer code obtained during this research is considerably robust, fast and applied; it can be used for many other axisymmetric complex geometries.

According to Table 1, the drag coefficient, as an important performance quantity, is reduced with a decrease in the belt angle. Also, for high belt angles, not only drag, but also lift coefficient is reduced due to flow separation downstream of the belt. Note that, as far as design is concerned, it is hard to make major conclusions, since we have only studied this problem from a certain point of view.

NOMENCLATURE

a	speed of sound
d	body diameter
L	body length
M	mach Number
x	longitudinal distance from the nose
z	perpendicular distance from the body surface
C_p	pressure coefficient
L/d	fineness ratio
α	angle of attack
θ	circumferential angle

REFERENCES

1. Fleeman, E.L. "Tactical missile design", *AIAA Education Series*, AIAA, New York (2001).
2. Cebeci, T. "Three dimensional boundary layer on missiles", *Tactical Missile Aerodynamics*, **104**, pp. 723-777 (1986).
3. Chin, S.S., *Missile Configurations Design*, McGraw-Hill (1965).
4. Soltani, M.R., Fazeli, H. and Farhanie, B. "Experimental investigations of aerodynamic behaviors of two wrap around fins", *Esteghlal Journal of Engineering, ISSN 1025-2851*, **21**(1), pp 141-152 (2002).
5. Perkins, E.W. and Jorgensen, L.H. "Comparison of experimental and theoretical normal-force distributions (including Reynolds number effects) on ogive-cylinder body at mach number 1.98", NACA-TN 3716 (1975).
6. Amdahl, D.J. "Interactive multi-block grid generation", *Numerical Grid Generation in Computational Fluid Mechanics*, S. Sengupta, J. Hauser, P.R. Eiseman

and J.F. Thompson, Eds., Pineridge Press, pp. 579-588 (1988).

7. Sorenson, R.L. and McCann, K.M. "A method for interactive specification of multiple-block topologies", *AIAA-91-0147* (1990).
8. Boerstoel, J.W., Jacobs, A., and Kassies, J.M., *Design and Testing*, Norway (1989).
9. Beam, R.M. and Warming, R.F. "An implicit factored scheme for the compressible Navier-Stokes equation", *AIAA J.*, **16**(4), pp. 393-402 (1978).
10. Masdari, M. "The flow study in the test section of the trisonic wind tunnel of Qadr research center", M.Sc. Thesis, Aerospace Engineering Dept., Sharif Univ. of Technology, Tehran, Iran (2003).
11. Bohbot, J., Bertin, D. and Darracq, D. "A conservative patched grid algorithm for turbulent flow computations of 3-D complex configurations", *European Congress on Computational Methods in Applied Sciences & Engineering, ECCOMAS 2000*, Barceiona, (Sept. 11-14, 2000).
12. Moore, F.G. "Approximation methods for weapon aerodynamics, progress in astronautics and aeronautics", *AIAA*, ISSN 1-56347-399-2, **186**, Reston, VA 20191-4344 USA (2000).
13. Soltani, M.R., Taiebi-Rahni, M., Farahani, M. and Heidari, M.R. "Flow measurements around a long axisymmetric body with varying cross section", *43rd AIAA Aerospace Sciences Meeting and Exhibit*, Reno, Nevada (Jan. 10-13, 2005).
14. Heidari, M.R., Soltani, M.R., Farahani, M. and Taeibi-Rahni, M. "Experimental investigations of supersonic flow around a long axisymmetric body", *Esteghlal Journal of Engineering*, ISSN 1025-2851, **24**(2), pp. 171-192 (2005).
15. Soltani, M.R., Taiebi-Rahni, M., Farahani, M. and Heidari, M.R. "Experimental investigations of surface pressure distributions and boundary layer profiles around a long axisymmetric body with varying cross sections", *IMECE2004*, Kuwait (2004).
16. Jorgensen, L.H. and Perkins, E.W. "Investigation of some wake vortex characteristics of an inclined ogive-cylinder body at Mach number 2", NACA-RM A55E31 (1955).